Title

Paleomagnetism and Ar-40/Ar-39 ages from volcanics extruded during the Matuyama and Brunhes Chrons near McMurdo Sound, Antarctica

Journal

Geochemistry Geophysics Geosystems, 5

ISSN

1525-2027

Authors

Tauxe, Lisa
Gans, P
Mankinen, E A

Publication Date

2004-06-01

Peer reviewed

Paleomagnetism and $^{40}Ar/^{39}Ar$ ages from volcanics extruded during the Matuyama and Brunhes Chrons near McMurdo Sound, Antarctica

Lisa Tauxe

Scripps Institution of Oceanography, University of California, San Diego

Phillip Gans

University of California, Santa Barbara

Edward A. Mankinen

U.S. Geological Survey, Menlo Park, California

Abstract. Maps virtual geomagnetic poles derived from international geomagnetic reference field models show large lobes with significant departures from the spin axis. These lobes persist in field models from the last few millenia. The anomalous lobes are associated with observation sites at extreme southerly latitudes. To determine whether these features persist for millions of years, paleomagnetic vector data from the continent of Antarctica are essential. We present here new paleomagnetic vector data and $^{40}Ar/^{39}Ar$ ages from lava flows spanning Brunhes and Matuyama Chrons from the vicinity of McMurdo Sound, Antarctica. Oriented paleomagnetic samples were collected from 50 lava flows by E. Mankinen and A. Cox in the 1965-1966 austral summer season. Preliminary data based largely on the natural remanent magnetization (NRM) directions were published by Mankinen and Cox [1988]. We have performed detailed paleomagnetic investigations of 37 sites with multiple fully oriented core samples to investigate the reliability of results from this unique sample collection. Of these, only one fails to meet our acceptance criteria for directional data. Seven are reversely magnetized. The mean normal and reverse directions are antipodal. The combined mean direction has $\bar{D} = 12, \bar{I} = -86, \alpha = 4, \kappa = 37$ and is indistinguishable from that expected from a GAD field. We obtained reproducible absolute paleointensity estimates from 15 lava flows with a mean dipole moment of 49 ZAm^2 and a standard deviation of 28 ZAm^2. $^{40}Ar/^{39}Ar$ age determinations were successfully carried out on samples from 18 of the flows. Our new isotopic ages and paleomagnetic polarities are consistent with the currently accepted geomagnetic reversal time scales.

Introduction

The structure of the geomagnetic field has been of interest ever since it was first realized that the geomagnetic field is essentially dipolar in nature (see translation of Gilbert's 1600 treatise, De Magnete [Price, 1958]). The fact that the field is not perfectly dipolar and that the non-dipolar part is constantly changing has also been known for centuries. Nonetheless, the assumption that, when averaged over sufficient time, the

geomagnetic field averages to that of a geocentric axial dipole (GAD) is central to much of paleomagnetic research. It is the nature of the non-GAD contribution to the geomagnetic field that has spurred continued interest in geomagnetism since Gilbert's first insight.

For the purpose of removing latitudinal dependence of the geomagnetic field vector, geomagnetic field elements declination, inclination and intensity (D, I, B) are frequently converted to the equivalent geocentric dipole source orientation (whose piercing point is the virtual geomagnetic pole position, VGP), and the virtual dipole moment (VDM). In Figure 1a we show VGP positions calculated from the directions evaluated at 500 uniformly distributed locations over Earth's surface from the international geomagnetic reference field (IGRF) of 1995. A GAD field would produce VGPs centered on the spin axis. While there are many VGPs clustered around the spin axis there are two prominent lobes of VGPs extending down over North America.

Constable [2003] showed that the source of these deviant poles becomes apparent when we contour the VGP latitudes observed over Earth's surface as illustrated in Figure 1b. Most of the deviant poles come from a restricted area in the southern Indian Ocean and on the eastern margin of Antarctica. Also shown is the location of the southernmost active volcano, Mt. Erebus in McMurdo Sound, Antarctica. In Figure 1c we show a contour plot of the associated intensities of the geomagnetic field. There are four prominent lobes, two in each hemisphere. The most intense southern hemisphere lobe, southeast of Australia is the location of the present magnetic south pole and is also the source of the most deviant VGPs. In most compilations of VGP latitude versus VDM (see e.g., Tanaka et al. [1995]), the most deviant VGPs are associated with the lowest VDMs. However, full vector data from high southern latitudes are non-existant. Therefore, the question arises as to how long lived these southern anomalies are and what time scales are required to average them out?

Historical documentation of geomagnetic field elements have been scoured to construct models for the evolution of the geomagnetic field over the last four hundred years (e.g., Bloxham and Jackson, 1992; Jackson et al., 2000). These models, when averaged over the time span of observation, suggest that at least some of the non-GAD features of the geomagnetic field are rather long lived. For example, VGPs calculated from directions drawn from the GUFM model (Jackson et al., 2000) and averaged over the last four centuries (see e.g., Figure 2a) are not centered on the spin axis but are concentrated in the easterly lobe of the two shown in Figure 1a. Moreover, the most deviant VGPs still come from the high southerly latitudes (Figure 2b). The time scale for models of geomagnetic field evolution is being steadily pushed back through the use of archeomagnetic and geological resources (e.g., Constable et al. 2000; Korte and Constable 2003) and now spans the last few millenia.

As we go back farther in time, the types of geomagnetic field models that can be constructed changes from "snap shots" of essentially instantaneous field states to statistical descriptions of the field (see e.g., Constable and Parker 1988). These types of models address the question of what distribution of geomagnetic field vectors is likely to be observed at specific locations around Earth. Early models of the field were concerned with the increase of scatter in the observations of VGPs as a function of latitude (e.g., Cox, 1962; McElhinny and Merrill 1975; McFadden et al., 1988).

There has been a surge of interest recently in the more general structure of the time averaged geomagnetic field, resulting in four new compilations of directional data: Quidelleur et al., (1994), Johnson and Constable (1996), Kelly and Gubbins (1997) and McElhinny and McFadden (1997). Because a better understanding of the long term behavior of the geomagnetic field requires data of the highest quality, paleomagnetists have begun the process of updating the paleomagnetic time averaged field database using more carefully controlled data sets (see e.g. Johnson et al., 1998; Carlut et al., 2000; Tauxe et al., 2000; Mejia et al. 2002; Tauxe et al. 2003; Brown et al. 2004).

Despite much effort, data from high latitudes, critical for a complete understanding of the geomagnetic field, are scarce. The paleosecular variation of recent lavas (PSVRL) database of McElhinny and McFadden (1997; MM97) includes a single reference to paleomagnetic sites from latitudes higher than 70° North or South. These data come from the continent of Antarctica: Mankinen and Cox (1988; MC88). MM97 assigned them a demagnetization code (DC) of 3, which implies that all samples were demagnetized using a blanket treatment the choice of which was justified through vector demagnetization diagrams. In fact, the data of MC88 are overwhelmingly the NRM directions supported by pilot samples with thorough demagnetization treatment. As such, they merit a demagnetization code of one. Such data, despite their obvious high quality, do not meet the minimum requirements for inclusion in many of the recent data compilations.

Databases such as PSVRL include directional data only, yet the intensity is a critical element of the ge-

omagnetic field. Although there has been substantial effort made at compiling and interpreting the intensity data (see e.g., Tanaka et al., 1995; Perrin and Shcherbakov 1997; Selkin and Tauxe, 2000; Biggin and Thomas 2003), no paleointensity data have been published for the last five million years from latitudes higher than 70° north or south.

Therefore, new data are essential for the purposes of constraining models of the distribution of geomagnetic field vectors at high latitudes and the associated VGPs and VDMs. We present here results from a reinvestigation of the Brunhes and Matuyama aged lava flows from McMurdo Sound, Antarctica.

Previous work in Antarctica

Mankinen and Cox (1988) published directions based on the NRMs from 50 lava flows from the vicinity of McMurdo Sound, collected in the 1965-1966 season. Eleven of these directions were based on oriented block samples; the rest were based on 303 separately oriented core samples drilled in the field from 39 lava flows. These were oriented both magnetically and by sighting of prominent geographic features.

Inspection of the α_{95} values for the multiple samples per lava flow ($N = 6 - 8$ in most cases) in the MC88 data set suggests a very high degree of reproducibility, ranging from 2 to 6°. The high latitude of the sampling sites combined with the excellent grouping of the NRM directions per site and demonstrated stability of the specimens during demagnetization suggest that, specimens from these samples will provide the high quality data required for a new class of time averaged field models.

We have obtained archived core samples from 37 of these lava flows for reanalysis. The locations of the sites studied here are shown in Figure 3 and are listed in Table 1. [Please note that we have renamed the sites "mcXX" for the MC88 map numbers; hence mc01 is the same as MC88's site number 1.]

Paleomagnetic Analyses

Paleodirections

We remeasured the NRMs from all specimens and found all but those from a single site (mc42) to be within a few degrees of the original NRMs. A total of 44 specimens, including at least one specimen from each site was subjected to step-wise alternating field demagnetization in the Sapphire Instruments SI-4 uniaxial AF demagnetizer at Scripps Institution of Oceanography. Beginning at 80 mT, specimens were subjected to a "double demagnetization" protocol whereby the specimen was first demagnetized along the x, y, z axis sequentially and measured. Then the specimen was demagnetized along $-x, -y, -z$ and remeasured. The two measurements were averaged. This procedure is used to detect the rare occurence of acquisition of anhysteretic remanence during the AF demagnetization procedure. In all but a few specimens, the two measurements were within about 5° of each other in these specimens. One specimen revealed large deviations of over 80°, however. A further 221 specimens were subjected to thermal demagnetization. Of these, 100 underwent a Thellier-Thellier experiment (Thellier and Thellier 1959) to obtain absolute paleointensity data. All paleomagnetic data have been submitted to the MAGIC online database at: http://earthref.org.

We plot the behavior of representative specimens during AF and thermal demagnetization in Figure 4. As stated by MC88, the specimens from McMurdo Sound are extremely well behaved. With only a very few exceptions, AF and thermal demagnetization both show linear decay to the origin. Characteristic components were determined using principal component analysis (Kirschvink 1980). Of the 265 specimens analyzed, 253 gave best-fit directions meeting the minimum requirements of having at least 4 consecutive demagnetization steps with a directions trending to the origin and a maximum angle of deviation (MAD) of $\leq 5°$. One specimen was fit with a best-fit plane and met the same criterion for acceptance. In Figure 5 we show the directions from specimens both before (Figure 5a,b) and after (Figure 5c,d) demagnetization. There is very little difference between the NRM directions and the characteristic components, for all but a few specimens.

Site mean directions were calculated using Fisher statistics (Fisher, 1953) using the characteristic directions. The single site with a great circle was treated using the technique of McFadden and McElhinny (1988) for combining best fit lines and planes. We list the site means in Table 1 and plot them along with their circles of 95% confidence in Figures 6a and b.

Tauxe et al. (2003) developed a methodology for assessing the consequences of using various selection criteria, such as the Fisher parameters k or α_{95} on the resulting distribution. Their method requires a large number of sites and the 36 presented here are insufficient for such a statistical approach. Nonetheless, the optimum criteria of $k \geq 100, N_{site} \geq 5$ found by Tauxe et al. (2003) appears to be reasonable for the McMurdo sound data set. In fact, only one site from the McMurdo

data set (mc42, which had only a single stable specimen direction, plotted as an "X" in Figure 6a) failed to meet these criteria.

Paleointensity

We subjected 95 specimens to the Coe variant of the Thellier-Thellier experiment (Coe et al. 1978) to determine paleointensity. In this experiment, the specimens were heated to a given temperature step and allowed to cool in zero field. After measuring this "zerofield" step, the specimens were heated to the same temperature and allowed to cool in a 40μT laboratory field applied along the specimen's "z" axis (in this case, along the length of the cylindrical specimens). After the 100, 200, 300, 400, 500, and 550° temperature steps, specimens were reheated to a lower temperature and allowed to cool in the laboratory field. The difference between the first in-field step and the second (the so-called partial thermal remanent magnetization (pTRM) check step) is a measure of changes in the specimen's capacity to carry a thermal remanence (TRM). An additional five specimens were subjected to a modified experiment (e.g., Riisager and Riisager, 2001) whereby after certain in-field steps, a second zero-field step was performed. The maximum difference between the first and the second steps (sometimes called the pTRM tail check) is a measure of the equivalence of the blocking and unblocking temperatures of partial thermal remanences. Representative examples of the Thellier-Thellier data are shown in Figure 7.

The key assumptions in a Thellier-Thellier experiment are that 1) the characteristic component of the NRM is a TRM and is linearly related to the ancient applied field, and 2) the acquisition of laboratory pTRMs is analogous to the original partial NRM acquisition. A number of factors can lead to a violation of either of these assumptions. For example, alteration either *in situ* or in the laboratory can violate the first and second assumptions respectively. If the unblocking of a given pTRM occurs at a different temperature than that at which it was blocked, the second assumption is violated and there will be a bias in the NRM/pTRM ratio resulting in an erroneous paleofield estimate.

The Thellier-Thellier experiment allows the calculation of any number of "quality control" parameters and a variety have been defined, such as Q of Coe et al. (1978). Q itself incorporates several other parameters such as f, the fraction of the NRM component used in the slope estimation, the "gap factor" which quantifies the distribution of temperature steps, σ the standard error of the slope (assuming uncertainty in both the pTRM and NRM data), and the absolute value of the best-fit slope $|b|$. The uncertainty of the slope is expressed by the quantity $\sigma/|b|$, a parameter we call β. Selkin and Tauxe (2000) summarized a somewhat different list of parameters, including the deviation of the angle that the NRM component used in the slope calculations makes with respect to the origin, the maximum angle of deviation of Kirschvink (1980) of that component, the pTRM difference ratio and so on. Because every study is somewhat different, there is no "magic bullet" set of parameters, no master β as it were, that will guarantee that the result is meaningful. In this study, we use the parameters defined by Tauxe and Staudigel (in press) to be useful in assessing the reliability of the data:

1. The origin test (Deviation ANGle or DANG of Tauxe and Staudigel [in press]) and the MAD of the component used in the slope calculation. MAD is calculated following Kirschvink (1980) and the deviation angle is the angle between the principal component of Kirschvink (1980) and the vector from the center of mass (see Kirschvink 1980) to the origin.

2. The "scatter" parameter (β).

3. We find that while remanence component fraction (f) works well with single component magnetizations and reflects the fraction of the total NRM used in the slope calculation, it is misleading when there are multiple components. We use therefore the fraction of the vector difference sum of the remanence (f_{vds}) defined by Tauxe and Staudigel [in press] which is the fraction of the total NRM, estimated by the vector difference sum (VDS) of the entire zero field demagnetization data. The VDS "straightens out" the various components of the NRM by summing up the vector differences at each demagnetization step. Because the data presented here are almost all single component NRMs, there is little difference between component fraction and the vector difference sum fraction. Nonetheless, we feel it wise to alert users of data that there is a difference and both parameters should be presented.

4. The difference between the original pTRM at a given temperature step (horizontal component of the circles in Figure 7) and the pTRM check (horizontal component of the triangles in Figure 7), δ_i, can result from experimental noise or from alteration during the experiment. Most papers pre-

senting paleointensity data require that the maximum pTRM difference to be 5% of the original pTRM. This allows the strongest pTRMs to have the largest deviations. Such a test would be sensible if measurement noise were inversely proportional to the magnitude of the pTRM. If anything, the opposite is true, but in most experiments, measurement noise is not the primary cause of scatter in the data. In order to "level the playing field" for pTRM checks, Selkin and Tauxe (2000) proposed to normalize the maximum pTRM difference value within the region of interest by the length of the hypotenuse of the NRM/pTRM data used in the slope calculation (the solid lines shown in Figure 7). Their Difference RATio is therefore the maximum difference ratio. In many cases, it is useful to consider the trend of the pTRM checks as well as their maximum deviations. If all the pTRM checks were positive for example, that might be an indication of growing alteration. Therefore the sum of these differences $\sum \delta_i$ is perhaps more useful than the maximum δ_i. Here, we normalize this difference sum by the pTRM acquired by cooling from the maximum temperature step used in the slope calculation to room temperature. This parameter is was callled the Difference RATio Sum (DRATS) by Tauxe and Staudigel [in press].

The behavior of the McMurdo Sound specimens, as characterized by the various quality parameters is illustrated in Figure 8. Most parameters show a clear inflection point separating "outlier" behavior from the rest. Inflections are marked for the pTRM difference ratio sums at about 30%, the fraction of the vector difference sum at 0.2, standard error of the slope at 0.1, the deviation angle at 10°, and maximum angle of deviation at 5°. Because there is no objective way of deciding the selection criteria for paleointensity data, we have chosen to use these inflection points as a guide for averaging at the site level. In addition, we have required there to be at least two pTRM checks prior to the maximum temperature step used and that the pTRM tail checks (where present) be less than 5%. We note that the complete data sethas been archived in the MagIC repository at earthref.org, so investigators can decide for themselves which criteria make the most sense in a different context. A total of 64 specimens from 25 sites meet these minimum criteria; we plot the paleofield estimates as both a histogram and a cumulative distribution in Figure 9.

Mean paleointensities were calculated for each site having specimens meeting the minimum criteria discussed above. These are listed in Table 2. The cumulative distribution of the standard deviations of replicate measurements expressed as a percentage of the mean ($100\sigma_B/B$) for sites with at least two specimens meeting the specimen criteria discussed above is plotted in Figure 8f. The inflection point is at about 15% so this is the cut-off taken for reliability at the site level. 15 sites meet this rather strict criterion. The mean and standard deviation of these 15 sites is 37 and 21 μT respectively translating to a mean dipole moment of mean and standard deviation of 49 and 28 ZAm^2 respectively.

^{40}Ar/^{39}Ar Analyses

Previous K-Ar dating of the McMurdo Volcanic Province by Armstrong et al. (1968), Treves (1968), Fleck et al. (1972), Forbes et al (1974) and Armstrong (1978) established the basic Tertiary and Quaternary volcanic history for the region. This work was distilled and summarized by Mankinen and Cox (1988) (MC88) in the course of their paleomagnetic investigation and helped guide their original site selection. We selected 18 samples from the sites analyzed paleomagnetically by MC88 for new age determinations by the ^{40}Ar/^{39}Ar incremental heating method in the geochronology laboratory at UCSB. Samples were selected based on their freshness, degree of crystallinity, and the level of uncertainty in their existing age assignment. In general, we focussed on those samples for which there was either no previous dating or for which the previous K-Ar dating yielded questionable or conflicting results. Most of the available samples are basalts (or alkaline equivalents of basalt) and thus lack a suitable high-K phenocryst phase. Our previous experience (e.g., Gans and Bohrson, 1998) demonstrates that excellent results can be obtained by ^{40}Ar/^{39}Ar incremental heating of groundmass concentrates from mafic lavas, provided care is taken to sample fresh rocks from the more slowly cooled interiors of flows that possess a holocrystalline groundmass. It is also advantageous to remove phenocryst phases such as olivine, pyroxene, and calcic plagioclase, which tend to have little or no potassium but are commonly reservoirs for excess argon. Our new ^{40}Ar/^{39}Ar results are generally more precise than the previous K-Ar ages and have provided some important new insights and refinements to the eruptive history of the McMurdo Volcanic Province, which we discuss below.

Analytical techniques

Splits of most of the original core samples collected by MC88 (not subjected to thermal demagnetization) were first carefully examined petrographically to determine which were sufficiently fresh and had the least amount of glass in the groundmass. Those deemed suitable for dating were lightly crushed and sieved to varying size fractions (100-200μm to 300-500μm, depending on the sample) and ultrasonically cleaned in de-ionized water. Standard magnetic separation techniques and hand picking were used to generate groundmass concentrates. Small un-irradiated splits of the purified samples were analyzed isotopically to determine their ^{40}Ar/mg and anticipated radiogenic yields, thus providing a preliminary age estimate and optimal target weight for each sample to be analyzed. Splits of each sample ranging from 50 to 200 mg were then encapsulated in copper packets and loaded into a sealed quartz vial interspersed with packaged flux monitors. Vials were irradiated in a cadmium-lined tube at the TRIGA reactor at Oregon State University in three separate irradiations for durations of 20 to 45 minutes depending on the estimated age of the sample. Upon return from the reactor and after sufficient time was allowed for undesirable short-lived isotopes to decay, the samples were then analyzed by incremental heating in a Staudacher-type resistance furnace using the general procedures and system described by Gans (1997). Analyses ranged from 8 to13 step heating experiments for each sample, focusing on the gas released between 600 and 1000°C, as this component of the gas generally has the highest radiogenic yields and is considered the most reliable. Our 19 new age determinations (on 18 samples) are summarized in Table 3 with selected age spectra and inverse isochron plots illustrated in Figures 10 and 11. All errors given for our estimated (preferred) ages as well on previous K-Ar ages as reported throughout the text and in Table 3 are $\pm$ 2 σ (95% confidence), and all older K-Ar ages have been recalculated for the new decay constants (Steiger and Jager, 1977). Complete data tables, age spectra, inverse isochron plots, and K/Ca plots are presented in Appendix 1. The flux monitor used for all irradiations was Taylor Creek Rhyolite with an assigned age of 27.92 Ma (Dalrymple and Duffield, 1988). For comparison, we obtain an age of 27.60 Ma on Fish Canyon Tuff Sanidine (another widely used standard) when we use 27.92 Ma Taylor Creek Rhyolite as our flux monitor.

Virtually all of the samples yielded well-behaved ^{40}Ar/^{39}Ar data with easily interpretable ages and uncertainties. Most of the samples yielded fairly flat age spectra having well defined plateaus or pseudo plateaus (Figure 10). Individual spectra range from "hump-shaped" to "U-shaped" to "L-shaped" - a range of spectral characteristics that is typical of these rock suites and is readily explainable in terms of the combined effects but variable contributions of reactor-induced recoil, low temperature argon loss, and a non-atmospheric "trapped" component (i.e. excess argon). In general, the flattest and most reliable parts of the individual spectra were associated with the gas released at intermediate temperatures. The anomalous apparent ages observed at low temperatures in some spectra are attributed to either reactor induced recoil (which tends to produce older apparent ages in the low temperature steps) or weathering/alteration induced argon loss in nature (which tends to produce younger ages). The old apparent ages in the high temperature steps for a number of the spectra is a common feature of whole rock age spectra and is typically associated with an abrupt drop in the apparent K/Ca ratios. We attribute these older ages to the outgassing of early crystallized and more refractory pyroxene, olivine, and/or calcic plagioclase which grew while the melt still resided at depth and trapped a non atmospheric argon component. Indeed, one of the principal advantages of the ^{40}Ar/^{39}Ar method is the ability to identify and separate these different reservoirs of argon and determine to what extent the data is meaningful. For example, a number of the samples gave total fusion ages (TFA = the age that would have been obtained had the sample been run in a single step) that were substantially older than the weighted mean plateau age (WMPA), on account of the older apparent ages associated with the high-temperature steps. The TFA is analogous to what would have been obtained in a conventional K-Ar age, and this discrepancy may explain why in a number of instances (e.g. samples mc01, mc09, mc35, mc39), the ages obtained by the ^{40}Ar/^{39}Ar method were slightly to significantly younger than the correlative K-Ar ages (see Table 3).

Hut Point Peninsula

Basalt lava flows and cones are exposed in close proximity to McMurdo Station and Scotts Base and throughout the Hut Point Peninsula. These deposits were previously divided into several informal sequences whose relative ages (from youngest to oldest) were inferred to be (1) Twin Crater, (2) Half Moon Crater, (3) Castle Rock, (4) Observation Hill, and (5) Crater Hill (Kyle and Treves, 1974). Only the Twin Crater Sequence was demonstrably Brunhes age, yielding normal polarity and K-Ar ages of 0.44 and 0.59 Ma (Armstrong,

1978). All of the other sequences were inferred to be older (Matuyama and perhaps Olduvai Chron) based on limited K-Ar dating and stratigraphic evidence (Armstrong, 1978, Kyle and Treves, 1974). Our new dating from the Hut Point Peninsula revises some of these age assignments and suggests that most of basaltic rocks on the Hut Point Peninsula are young (Brunhes Chron).

The trachytes of Observation Hill are the only demonstrably older (Matuyama) flows on the Hut Point Peninsula, with reversed polarity and previous K-Ar ages of 1.22 to 1.28 Ma (Forbes et al, 1974). We dated mc01 from the north flank of Observation Hill and obtained a well-behaved plateau age of 1.18 ± 0.01 Ma, in good agreement with the previous results (Figure 10). Samples mc02 and mc03 both belong to the Crater Hill sequence that had previously been interpreted as the oldest sequence on the peninsula because basalts included within this sequence are locally overlain by trachyte flows of Observation Hill (Kyle and Treves, 1974). However, MC88 questioned this interpretation, given the normal polarity of most Crater Hill lavas and difficulties in assigning them an age as old as Olduvai. Our new dates of 0.33 ± 0.02 and 0.348 ± 0.008 on Crater Hill sequence basalts confirms MC88s suspicions and suggest the Crater Hills sequence is amongst the youngest basalts on the peninsula. A dike from Fortress Rock (mc04) yielded an age of 0.340 ± 0.006 Ma, in general agreement with other ages from the Twin Crater sequence and suggests that the Crater Hill and Twin Crater sequences are broadly coeval (∼330 550 ka). In the northeast part of the Hut Point Peninsula, The Half Moon Crater, Castle Rock (mc07), and Breached Cone areas (mc08) had yielded normal polarities but the only previous K-Ar age determinations of 1.0 ± 0.2 and 1.1± 0.4 (Kyle and Treves, 1974) indicated that they ought to be reverse or perhaps lie within the Jaramillo or Cobb Mountain Normal Polarity subchrons. We obtained a plateau age of 0.65 ±0.05 Ma from a basalt flow at Breached Cone (mc08). This new age, together with the evidence for incorporation of excess argon as indicated by its U-shaped spectrum, suggests that most of the volcanic rocks from the northeastern Hut Point Peninsula also belong in the Brunhes Chron and that the older K-Ar ages may not be reliable.

Cape Royds and Cape Evans

The capes on the west side of Ross Island are underlain mainly by kenyte and anorthoclase trachyte flows derived from Mount Erebus. The only previous K-Ar dating of kenyte flows from this region yielded ages of 0.70 and 0.97 Ma but normal polarities. Three major kenyte flows are exposed at Cape Royds (Smith, 1954), the middle one having yielded an age of 0.70 ± 0.14 Ma (Treves, 1962). We dated one of these kenyte flows (mc09) and obtained a much younger age (74 ± 15 ka). Presumably this is the youngest of three flows, but the > 0.5 Ma age difference is still surprising. A 12-meter high kenyte flow from the tip of Cape Evans also yielded a very young age (55 ± 10 ka). Without more work, it is not clear whether the kenyte flows in these areas were erupted over a prolonged period spanning the last 1 Ma, or whether the older K-Ar ages should be considered suspect.

Cape Crozier and Dailey Island

Both basalts and trachyte flows are widely exposed on Cape Crozier and have generally yielded reverse polarities (MC88). We re-dated the trachyte of Post Office Hill (mc15) and obtained an excellent plateau age of 1.33 ± 0.02 Ma, in good agreement with the previous K-Ar date of 1.35 Ma by Armstrong (1978). No previous dates had been obtained from Dailey Island but all of the previously measured polarities are normal. We obtained a somewhat U-shaped spectrum with an interpreted age of 0.77 ± 0.04 Ma on a dike cutting a youthful looking cone (mc20), suggesting that these volcanic centers belong to the older part of the Brunhes Chron.

Mount Morning

Mount Morning was interpreted to be the youngest of the volcanic fields investigated by MC88, with 13 of their 14 sites yielding normal polarities. The volcanic rocks on the northeast flank of Mount Morning were deposited over the remnants of a much older volcanic edifice, including a dike that yielded an age of 15.4 ± 0.5 Ma (Armstrong, 1978). A single age of 0.28± 0.04 Ma was reported by MC88, though not on one of their paleomagnetic samples. We obtained ages of 4.47 ± 0.04, 0.28 ± 0.02, 0.12 ± 0.02, and 0.084 ± 0.008 Ma on different olivine basalt flows from various parts of the field. The relative ages of the younger flows were as predicted by MC88 based on their degree of weathering, and confirm the overall youthfulness of this volcanic field. The older age of 4.47 Ma was obtained from a deeply dissected cone in the eastern part of the field.

Mount Discovery

No previous dates had been obtained from the Mount Discovery samples of MC88, though Armstrong (1978) reported a 5.3 ±0.1 Ma K-Ar age on feldspar from basalt at the summit of Mount Discovery. We obtained

ages of 0.084 ± 0.008 on an olivine basalt flow (mc28) and 0.12 ± 0.02 on a basalt dike cutting a youthful cone (mc29), consistent with their youthful appearance and normal polarity (Brunhes Chron).

Walcott Bay

Previous work in the Walcott Bay Roaring Glacier region had yielded both normal and reverse polarities and K-Ar ages on basalt flows that ranged from 2.16 to 0.2 Ma (Armstrong, 1978). We dated two of the MC88 samples olivine basalt from the terminus of Walcott Glacier (mc47), which yielded an age of 1.14 ± 0.02 Ma, and olivine basalt from Roaring Valley (mc50), which yielded an age of 1.90 ± 0.1 Ma. Both of these ages are consistent with their reverse polarity (Matuyama) and fall within the range of ages documented by Armstrong (1978).

Discussion

We now have a robust and reasonably well dated set of directional data from 36 sites and intensity data from 15 sites spanning the last 5 million years from a high southerly latitude (∼ -78°). Averages of normal, reverse and combined directions and associated paleopoles are listed in Table 4 along with mean field intensity and axial dipole moment (ADM).

Of the 36 sites that yielded meaningful site mean directions, seven are reversely magnetized. The confidence bounds of the antipode of the mean reverse direction includes the mean normal direction (see Figure 6c), hence the normal and reverse sites are antipodal at the 95% level of confidence. The grand mean directions are distinct from the present field direction (triangle in Figure 6c), but indistinguishable from the direction expected from a GAD field (see Table 4).

Two issues raised in the introduction were the persistence of lobes of non-axial VGPs and scatter of VGPs at high latitude. We address both of these in Figure 12. The VGP positions for sites listed in Table 1 (excluding mc42) are shown in the inset. As expected from the coincidence of the mean directions with that predicted by a GAD field, the VGPs scatter about the spin axis and are not significantly deflected as in the present field. The scatter of the VGPs, according to the methods set out in MM97 is $S = 21.1^{25.1}_{16.5}$, using Vandamme's (1994) criteron for excluding low north or south latitude VGPs of 48.3° or less. We use the same procedure for determining the VGP cut-off value in order to facilitate comparison with MM97's estimates for scatter with respect to latitude using the global data set. The estimates for scatter S of MM97 are shown in Figure 12. The estimate for S for the McMurdo data is plotted as a square. It is probable that 36 VGPs are too few to allow a robust estimate for scatter, yet it appears that the scatter from this high latitude study is consistent with the global trends.

Another issue raised in the introduction was the lack of paleointensity data for high latitudes in any of the recent compilations for the last 5 million years. The present dipole moment of Earth's magnetic field is approximately 80 ZAm^2. Until recently, this was thought to approximatel the average dipole moment (Merrill et al. 1996). However, better data selection criteria as well as a number of new data points meeting high experimental standards led Selkin and Tauxe (2000) to suggest that the average for the last 5 million years was substantially lower than the present dipole moment, or approximately 45 ZAm^2.

There are no paleointensity data from latitudes higher than 70° north or south in the published literature for this time period, so the data presented here constitute a test for the average suggested by Selkin and Tauxe (2000). In Figure 13 we plot the data compiled by Selkin and Tauxe (2000) for the time period 0.3-5 Ma as solid symbols and the intensity expected from the 5 million year average (solid line) as well as that expected from the present dipole moment (dashed line). Our new data from McMurdo sound are plotted as open symbols. The average McMurdo Sound paleofield estimate is virtually identical to that predicted by the Selkin and Tauxe (2000) average dipole moment (45 ZAm^2), and incompatible with that expected from the present dipole moment (80 ZAm^2).

Conclusions

We present new paleomagnetic and geochronological data from the sample collection of Mankinen and Cox (1988) from McMurdo Sound, Antarctica. These meet the standards for modern studies. The directional data are virtually identical to those published by Mankinen and Cox (1988) based on NRM measurements and attest to the high degree of paleomagnetic stability of the McMurdo Sound lava flows. The directions yield 36 site means with $\kappa \geq 100, N_{site} \geq 5$, seven of which are reversely magnetized. The normal and reverse data are antipodal and the means are indistinguishable from those expected from a geocentric axial dipole. The scatter of the associated VGPs is also compatible with that predicted from the global compilations of McElhinny and McFadden (1997). Paleointensity estimates of 16

sites meeting our acceptance criteria yield and estimate of the mean and standard deviation of the dipole moment (49 and 28 ZAm^2 respectively) indistinguishable from the estimate of Selkin and Tauxe (2000) of 45 ZAm^2 for the last 5 million years.

Acknowledgements. This work was supported by NSF EAR 9805164 to LT and PG. We are grateful for helpful conversations with Cathy Constable, Peter Selkin and Catherine Johnson. Also, we thank Sherm Grommè, Laurie Brown, Victoria Mejia and Cathy Constable for thorough and thoughtful reviews.

References

Armstrong, R., K-Ar dating: Late Cenozoic McMurdo Volcanic Group and dry valley glacial history, Victoria Land, Antarctica, *N.Z. J. Geol. Geophys.*, *21*, 685–698, 1978.

Armstrong, R., W. Hamilton, and G. Denton, Glaciation in Talor Valley, Antarctica, older than 2.7 million years, *Science*, *159*, 187–189, 1968.

Biggin, A. J., and D. N. Thomas, Analysis of long-term variations in the geomagnetic poloidal field intensity and evaluation of their relationship with global geodynamics, *Geophys. J. Int.*, *152*, 392–415, 2003, 635WX GEOPHYS J INT.

Bloxham, J., and A. Jackson, Time-dependent mapping of the magnetic field at the core-mantle boundary, *J. Geophys. Res.*, *97*, 19,537–19,563, 1992.

Brown, L., B. Singer, and M. Gorring, Paleomagnetism and $^{40}Ar/^{39}Ar$ chronology of lavas from Meseta del Lago Buenos Aires, Patagonia, *Geochem., Geophys., Geosyst.*, *5*, Q01H04, doi:10.1029/2003GC000,526, 2004.

Carlut, J., X. Quidelleur, V. Courtillot, and G. Boudon, Paleomagnetic directions and K/Ar dating of 0 to 1 Ma lava flows from La Guadeloupe Island (French West Indias): Implications for time-averaged field models, *J. Geophys. Res.*, *105*, 835–849, 2000.

Coe, R. S., S. Grommé, and E. A. Mankinen, Geomagnetic paleointensities from radiocarbon-dated lava flows on Hawaii and the question of the Pacific nondipole low, *J. Geophys. Res.*, *83*, 1740–1756, 1978.

Constable, C., and R. L. Parker, Statistics of the geomagnetic secular variation for the past 5 m.y., *J. Geophys. Res.*, *93*, 11,569–11,581, 1988.

Constable, C. G., Geomagnetic reversals: rates timescales, preferred paths, statistical models and simulations, in *Earth's Core and Lower Mantle*, edited by C. Jones, A. Soward, and K. Zhang, The Fluid Mechanics of Astrophysics and Geophysics, Taylor and Francis, London, 2003.

Constable, C. G., C. L. Johnson, and S. P. Lund, Global geomagnetic field models for the past 3000 years: transient or permanent flux lobes?, *Phil. Trans. Roy. Soc. London, Series A*, *358*, 991–1008, 2000.

Cox, A., Analysis of present geomagnetic field for comparison with paleomagnetic results, *J. Geomag. Geoelectr.*, *13*, 101–112, 1962.

Dalrymple, G., and W. Duffield, High-precision $^{40}Ar/^{39}Ar$ dating of Oligocene rhyolites from the Mogollon-Datil volcanic field using a continuous laser system, *Geophys. Res. Lett.*, *15*, 1988.

Fisher, R. A., Dispersion on a sphere, *Proc. Roy. Soc. London, Ser. A*, *217*, 295–305, 1953.

Fleck, R., L. Jones, and R. Behling, K-Ar dates of the McMurdo volcanics and their relation to the glacial history of Wright Valley, *Antarct. J. U.S.*, *7*, 244–246, 1972.

Forbes, R., D. Turner, and J. Carden, Age of trachyte from Ross Island, *Geology*, *2*, 1974.

Gans, P., Large-magnitude Oligo-Miocene extension in southern Sonora - implications for the tectonic evolution of northwest Mexico, *Tectonics*, *16*, 388–408, 1997.

Gans, P., and W. A. Bohrson, Suppression of volcanism during rapid extension in the Basin and Range Province, United States, *Science*, *279*, 66–68, 1998.

Jackson, A., A. R. T. Jonkers, and M. R. Walker, Four centuries of geomagnetic secular variation from historical records, *Phil. Trans. Roy. Soc. London, Series A*, *358*, 957–990, 2000.

Johnson, C. L., and C. G. Constable, Palaeosecular variation recorded by lava flows over the past five million years, *Phil. Trans. R. Soc. Lond. A.*, *354*, 89–141, 1996.

Johnson, C. L., J. R. Wijbrans, C. G. Constable, J. Gee, H. Staudigel, L. Tauxe, V. H. Forjaz, and M. Salgueiro, $^{40}Ar/^{39}Ar$ ages and paleomagnetism of Sao Miguel lavas, Azores, *Earth Planet. Sci. Lett.*, *160*, 637–649, 1998.

Kelly, P., and D. Gubbins, The geomagnetic field over the past 5 million years, *Geophys. J. Int.*, *128*, 315–330, 1997.

Kirschvink, J. L., The least-squares line and plane and the analysis of paleomagnetic data, *Geophys. Jour. Roy. Astron. Soc.*, *62*, 699–718, 1980.

Korte, M., and C. G. Constable, Continuous global geomagnetic field models for the past 3000 years, *Phys. Earth Planet. Inter.*, *140*, 73–89, 2003.

Kyle, P., and S. Treves, Geology of Hut Point Peninsula, Ross island, *Antarct. J. U.S.*, *9*, 232–234, 1974.

Mankinen, E., and A. Cox, Paleomagnetic investigation of some volcanic rocks from the McMurdo volcanic province, Antarctica, *J. Geophys. Res.*, *93*, 11,599–11,612, 1988.

McElhinny, M. W., and P. L. McFadden, Palaeosecular variation over the past 5 Myr based on a new generalized database, *Geophys. J. Int.*, *131*, 240–252, 1997.

McElhinny, M. W., and R. T. Merrill, Geomagnetic secular variation over the past 5 m.y, *Rev. Geophys. Space Phys.*, *13*, 687–708, 1975.

McFadden, P. L., and M. W. McElhinny, The combined analysis of remagnetization circles and direct observations in paleomagnetism, *Earth Planet. Sci. Lett.*, *87*, 161–172, 1988.

McFadden, P. L., R. T. Merrill, and M. W. McElhinny, Dipole/Quadrupole family modeling of paleosecular variation, *J. Geophys. Res*, *93*, 11,583–11,588, 1988.

Mejia, V., R. Barendregt, and N. Opdyke, Paleosecular variation of Brunhes age lava flows from British Columbia, Canada, *Geochem., Geophys., Geosyst.*, *3*, DOI number 10.1029/2002GC000,353, 2002.

Merrill, R. T., M. W. McElhinny, and P. L. McFadden, *The Magnetic Field of the Earth: Paleomagnetism, the Core, and the Deep Mantle*, Academic Press, 1996.

Perrin, M., and V. Shcherbakov, Paleointensity of the Earth's magnetic field for the past 400 Ma: evidence for a dipole structure during the Mesozoic low, *J. Geomag. Geoelectr.*, pp. 601–614, 1997.

Price, D., *William Gilbert and his De Magnete*, Basic Books, Inc., New York, 1958.

Quidelleur, X., J. P. Valet, V. Courtillot, and G. Hulot, Long-term geometry of the geomagnetic field for the last five million years: An updated secular variation database, *Geophys. Res. Lett.*, *21*, 1639–1642, 1994.

Riisager, P., and J. Riisager, Detecting multidomain magnetic grains in Thellier palaeointensity experiments, *Phys. Earth Planet. Int.*, *125*, 111–117, 2001, 479WX PHYS EARTH PLANET INTERIORS.

Selkin, P., and L. Tauxe, Long-term variations in paleointensity, *Phil. Trans. Roy. Astron. Soc.*, *358*, 1065–1088, 2000.

Smith, W., The volcanic rocks of the Ross Archipelago: British Antarctic ("Terra Nova") Expedition, 1910, *Nat. Hist. Rep. Geol.*, *2*, 1–107, 1954.

Steiger, R. H., and E. Jager, Subcommission on geochronology: Conventions on the use of decay constants in geo- and cosmochronology, *Earth Planet. Sci. Lett.*, *36*, 359–362, 1977.

Tanaka, H., M. Kono, and H. Uchimura, Some global features of paleointensity in geological time, *Geophys. J. Int.*, *120*, 97–102, 1995.

Tauxe, L., and H. Staudigel, Strength of the geomagnetic field in the Cretaceous Normal Superchron: New data from submarine basaltic glass of the Troodos Ophiolite, *Geochem., Geophys., Geosyst.*, in press.

Tauxe, L., H. Staudigel, and J. Wijbrans, Paleomagnetism and $^{40}Ar/^{39}Ar$ ages from La Palma in the Canary Islands, *Geochem., Geophys., Geosyst.*, *1*, doi:2000GC000,063, 2000, in press.

Tauxe, L., C. Constable, C. Johnson, W. Miller, and H. Staudigel, Paleomagnetism of the Southwestern U.S.A. recorded by 0-5 Ma igneous rocks, *Geochem., Geophys., Geosyst.*, p. DOI 10.1029/2002GC000343, 2003.

Thellier, E., and O. Thellier, Sur l'intensité du champ magnétique terrestre dans le passé historique et géologique, *Ann. Geophys.*, *15*, 285–378, 1959.

Treves, S., The geology of Cape Evans and Cape Royds, ross Island, Antarctica, in *Antarctic Research: The Matthew Fontaine Maury Memorial Symposium: Geophys. Monogr. Ser.*, edited by H. Wexler, M. rubin, and J. Caskey, vol. 7, pp. 108–109, Amer. Geophys. Union, Washington, D.C., 1962.

Treves, S., Volcanic rocks of the Ross Island area, *Antarct. J. U.S.*, *3*, 108–109, 1968.

L. Tauxe, Scripps Institution of Oceanography, La Jolla, CA 92093-0220, USA (e-mail: ltauxe@ucsd.edu); Phillip Gans, Dept. Geological Science, University of California Santa Barbara, Santa Barbara, CA 93106-9630 (e-mail: gans@magic.ucsb.edu); E.A. Mankinen, US Geological Survey, MS 937, 345 Middlefield Rd, Menlo Park, CA 94025-3561, (e-mail: emank@usgs.gov)

This preprint was prepared with AGU's LaTeX macros v4, with the extension package 'AGU^{++}' by P. W. Daly, version 1.6b from 1999/08/19.

Table 1. Average directions by site from the McMurdo sample collection.

Site	Site Lat. (N)	Site Long. (E)	I	D	α_{95}	N_l	N_p	κ	Pol.	VGP Lat.	VGP Long.
mc01	-77.85	166.64	77.7	250.4	4.3	7	0	199.2	R	-67.6	86
mc02	-77.85	166.69	-81.3	324.4	3.4	6	0	389.4	N	80	87.1
mc03	-77.84	166.76	-82.2	350.3	2.8	6	0	563.3	N	86.1	125.9
mc04	-77.84	166.7	-86.1	328.2	5.5	5	0	196.9	N	83.1	23.1
mc06	-77.83	166.67	-78.8	13.6	4.8	5	0	254.4	N	79.8	196
mc07	-77.8	166.72	-69.1	156.8	3.2	5	0	570.9	N	41.2	328.2
mc08	-77.8	166.83	-78.3	38.5	2.7	8	0	430.5	N	75.1	234.6
mc09	-77.55	166.2	-82.7	258	3.7	8	0	220.5	N	69.2	29.3
mc10	-77.57	166.23	-78.6	335.2	4.1	8	0	183.9	N	78.2	116.3
mc11	-77.57	166.23	-77.1	327	2.2	8	0	623.1	N	74.4	108.9
mc13	-77.64	166.41	-71.6	117	5	8	0	122.9	N	49.4	297.1
mc14	-77.46	169.23	-80.8	0.5	2.7	8	0	436.1	N	84.6	170.9
mc15	-77.47	169.23	83.9	173.4	2.3	8	0	569.7	R	-88.5	237.7
mc19	-77.86	165.23	-80.5	146.3	4.9	7	0	151.2	N	60.6	324.2
mc20	-77.88	165.02	-77.3	141.6	4.5	6	0	226.9	N	55.5	318.3
mc21	-78.21	166.49	79.3	329.7	3.2	8	0	309.1	R	-58.6	146.5
mc26	-78.21	166.57	-57.4	9.3	4.8	8	0	134.8	N	49.6	177.9
mc28	-78.29	164.73	-82.1	92	4.9	6	0	188	N	70.3	292.2
mc29	-78.31	164.8	-76.6	9.4	5.3	8	0	109.8	N	75.9	181.6
mc30	-78.34	164.87	68.1	242.1	4.8	8	0	133.8	R	-55.3	61.7
mc31	-78.34	164.28	-86.1	298.3	3.1	5	0	602.3	N	79.5	25.1
mc32	-78.36	164.3	-74.6	265.1	3.3	7	0	343.7	N	58.2	50
mc33	-78.38	164.34	-75.5	9.7	3	8	0	343.2	N	74	180.6
mc34	-78.39	164.27	-82	280.1	3.4	7	0	319	N	72.3	45.3
mc35	-78.39	164.23	-84.2	293.9	3.3	8	0	280.2	N	77.5	41.2
mc36	-78.39	164.27	-82.8	344.7	4.8	7	0	159.5	N	85.7	103.6
mc37	-78.4	164.27	81.7	212.1	3	8	0	333.5	R	-81.1	59.4
mc38	-78.4	164.21	-78	296.6	4	7	0	224.2	N	69.5	72
mc39	-78.39	164.21	-85.9	264.3	4.2	7	1	178.1	N	75.2	17.8
mc40	-78.39	164.2	-83.2	192.8	5.1	7	0	139.1	N	65.1	351.2
mc41	-78.39	164.12	-80	260.6	4.4	5	0	305.9	N	65.9	37.6
mc42	-78.37	164.12	-29.9	84.3	0	1	0	0	X	16.9	251.9
mc43	-78.37	164.24	-89.1	282.1	5.4	6	0	153.7	N	78.6	353.2
mc44	-78.36	164.26	-73.9	324.2	4.5	8	0	152.5	N	68.4	111.5
mc48	-78.24	163.36	-55.7	75.3	4.5	6	0	219.3	N	38.4	247.5
mc49	-78.24	163.36	74.3	147.9	3.2	5	0	580	R	-69.7	294.7
mc50	-78.25	163.22	71.4	191.4	2.6	8	0	468.6	R	-67.5	360

$\bar{I}, \bar{D}$ are mean inclination and declination respectively. α_{95} is the Fisher (1953) circle of 95% confidence. N_l, N_p are the number of best-fit lines and planes respectively of all specimens interpreted. κ is an estimate of the Fisher (1953) precision parameter. Pol. is the designated polarity: N is normal, R is reverse and X is uninterpreted. VGP Lat., Long. is the location of the virtual geomagnetic pole calculated for the site.

Table 2. Summary of paleointensity results.

Site	N_B	$B(\mu T)$	σ_B	$100\times\sigma_B/B$	VADM (ZAm^2)	σ_{VADM}
mc01	2	18.4	2.1	11.5	24.2	2.8
mc08	4	50.9	5.6	11.1	66.8	7.4
mc09	2	27.5	0.6	2.3	36.1	0.8
mc10	1	41.2	0	0	54.1	0.0
mc11	4	39.2	15.3	39	51.5	20.1
mc13	3	28.8	3.3	11.3	37.8	4.3
mc14	2	100.7	12.4	12.4	132.3	16.3
mc15	3	29.7	2.3	7.8	39.0	3.0
mc19	1	24.6	0	0	32.3	0.0
mc21	4	45.3	2.9	6.4	59.4	3.8
mc26	4	12	0.6	5.4	15.7	0.8
mc28	2	7.2	1.4	19.6	9.4	1.8
mc30	4	39	0.7	1.9	51.1	0.9
mc32	3	29.8	2.1	7	39.1	2.8
mc33	1	33	0	0	43.3	0.0
mc34	1	26.5	0	0	34.7	0.0
mc35	4	26	2.9	11.1	34.1	3.8
mc36	3	25.4	3.5	13.6	33.3	4.6
mc37	4	59.6	4.9	8.2	78.1	6.4
mc38	1	46.3	0	0	60.7	0.0
mc39	2	27.2	1.7	6.2	35.6	2.2
mc40	1	39.4	0	0	51.6	0.0
mc44	4	25.1	11.2	44.6	32.9	14.7
mc48	1	15	0	0	19.7	0.0
mc50	3	37.2	4.7	12.6	48.8	6.2

N_B is the number of specimens with a grade of "A". $\bar{B}(\mu T)$ is the average field strength. σ_B is the standard deviation of replicate specimens. $100\times\sigma_B/\bar{B}$ is the percent of σ_B of the average field strength. VADM (ZAm^2) is the Virtual Axial Dipole moment and Z is 10^{21}. σ_{VADM} is the standard deviation of the replicate specimens.

Table 3. Summary of $^{40}Ar/^{39}Ar$ results. Details of analyses are in the Appendix.

Sample	Mat.	Pref. Age (Ma)	TFA	WMPA	IsoA	K-Ar Age*	Polarity
mc01	WR	1.18 ± 0.01	1.17	1.182±0.008	1.19±0.02	1.25±0.06	R
mc02	WR	0.33 ± 0.02	0.336	0.320±0.014	0.338±0.042	na	N
mc03	WR	0.348 ± 0.008	0.683	0.348±0.008	0.342±0.016	na	N
mc04	WR	0.34 ± 0.006	0.333	0.340±0.006	0.338±0.012	na	N
mc08	WR	0.65 ± 0.05	0.732	0.647±0.040	0.656±0.062	na	N
mc09	WR	0.074 ± 0.015	0.071	0.063±0.004	0.068 ±0.014	0.70±0.14	N
				0.085±0.006	0.084±0.024		
mc13	WR	0.055 ± 0.01	0.051	0.056±0.004	0.050±0.022	na	N
mc15	PLAG	1.33 ± 0.05	1.31	1.32±0.02	1.33±0.04	1.35±0.08	R
mc15	WR	1.33 ± 0.02	1.33	1.33±0.02	1.33±0.04	1.35±0.08	
mc20	WR	0.77 ± 0.032	1.02	0.770±0.032	0.758±0.052	na	N
mc28	WR	0.06 ± 0.006	0.05	0.060±0.006	0.064±0.008	na	N
mc29	WR	0.18 ± 0.08	0.34	0.187±0.056	0.181±0.080	na	N
mc35	WR	0.12 ± 0.02	0.137	0.117±0.014	0.134±0.30	∼0.28±0.08	N
mc36	WR	0.12 ± 0.02	0.313	0.118±0.016	0.126+0.034	0.28±0.08	N
mc37	WR	4.47 ± 0.04	4.32	4.47±0.04	4.47±0.08	na	R
mc39	WR	0.084 ± 0.008	0.152	0.084±0.008	0.073±0.032	0.28±0.08	N
mc41	WR	0.28 ± 0.02	0.324	0.281±0.018	0.290±0.038	na	N
mc49	WR	1.14 ± 0.02	1.14	1.14±0.02	1.14±0.04	1.49±0.30	R
mc50	WR	1.9 ± 0.1	1.58	1.91±0.06	1.90±0.16	0.92 ±0.18	R

*MC88, Mat. - materials analyzed (WR = groundmass concentrates from whole rock samples, PLAG = plagioclase) Pref. Age (Ma) = Our preferred age in millions of years. TFA = total fusion age (age that would be obtained from integrating the entire spectrum) WMPA = weighted mean plateau age IsoA = Inverse isochron age, All uncertainties are 2 σ (95% confidence) in Ma

Table 4. Grand means for McMurdo Sound data.

Type of average	I	D	α_{95}	N	κ	PP Lat.	PP Long.	A_{95}
Mean normal paleopole	-86.2	359.3	4.5	29	36.5	85.2	355.1	8.1
Mean reverse paleopole	81.2	215.4	9.2	7	43.6	-80.6	64.8	17.4
Grand mean paleopole	85.4	12.0	4.0	36	37.4	-86.3	147	7.2
Present direction	-81.1	148.9						
GAD direction	-83.9	0						
		N	B (μT)	σ_B	ADM (ZAm^2)	σ_{ADM}		
Grand mean intensity	& dipole moment:	16	34.8	18.1	46.3	28.9		

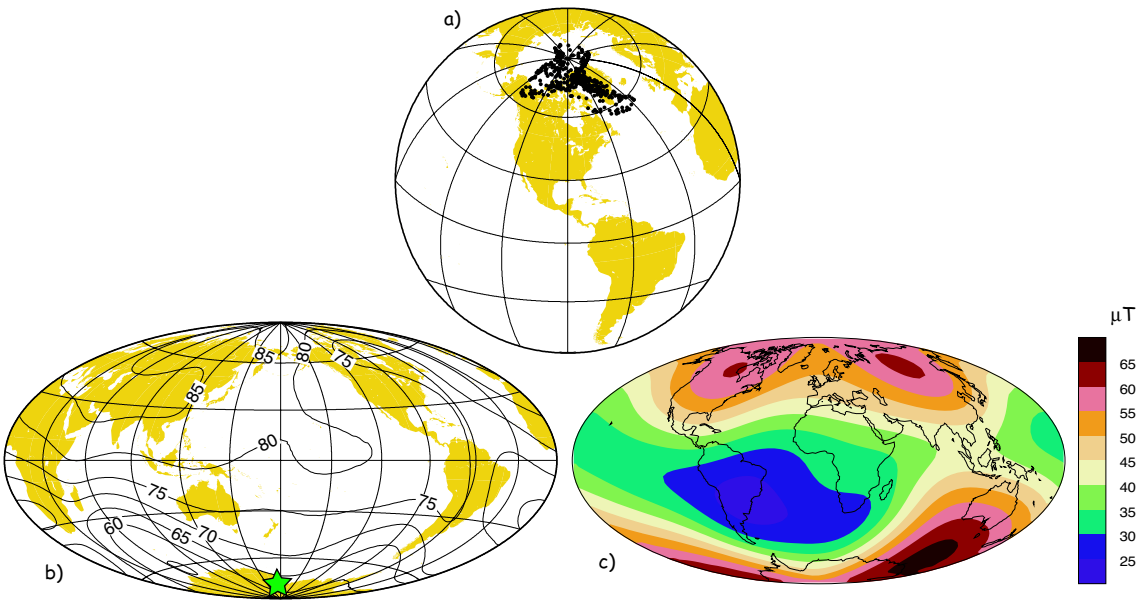

Figure 1. Key features of the 1995 International Geomagnetic Reference Field. a) Virtual geomagnetic pole positions from 500 locations around the globe. b) Contour plot of VGP latitude as a function of position. The most extreme VGP positions come from a swath of locations extending from Antarctica to the Southeast Indian Ocean. The location of McMurdo Sound is shown as the star. c) Contour of intensity estimates from IGRF 1995. There are two anomalous regions in the northern hemisphere and southern hemispheres each, one centered on McMurdo Sound.

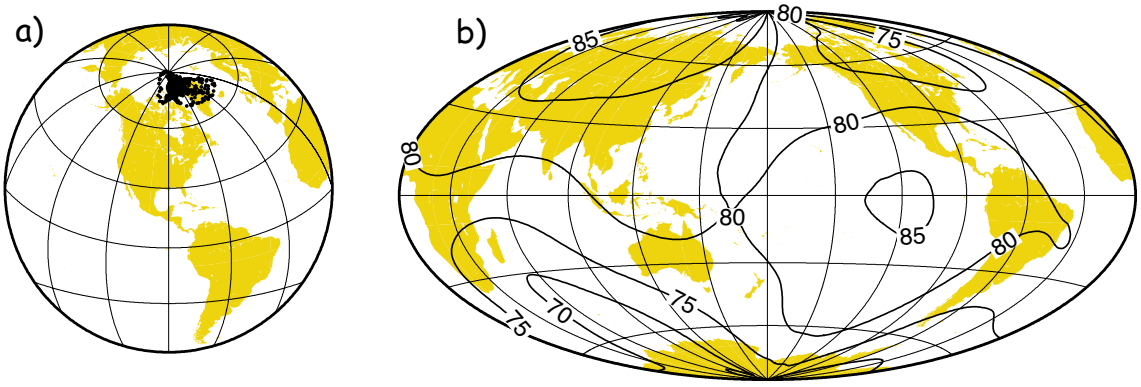

Figure 2. a) VGPs calculated from 400 year averages of directions drawn from the GUFM model of Jackson et al. (2000) at distributed locations around Earth. b) Contours of observed VGP latitude at the observations sites used in a).

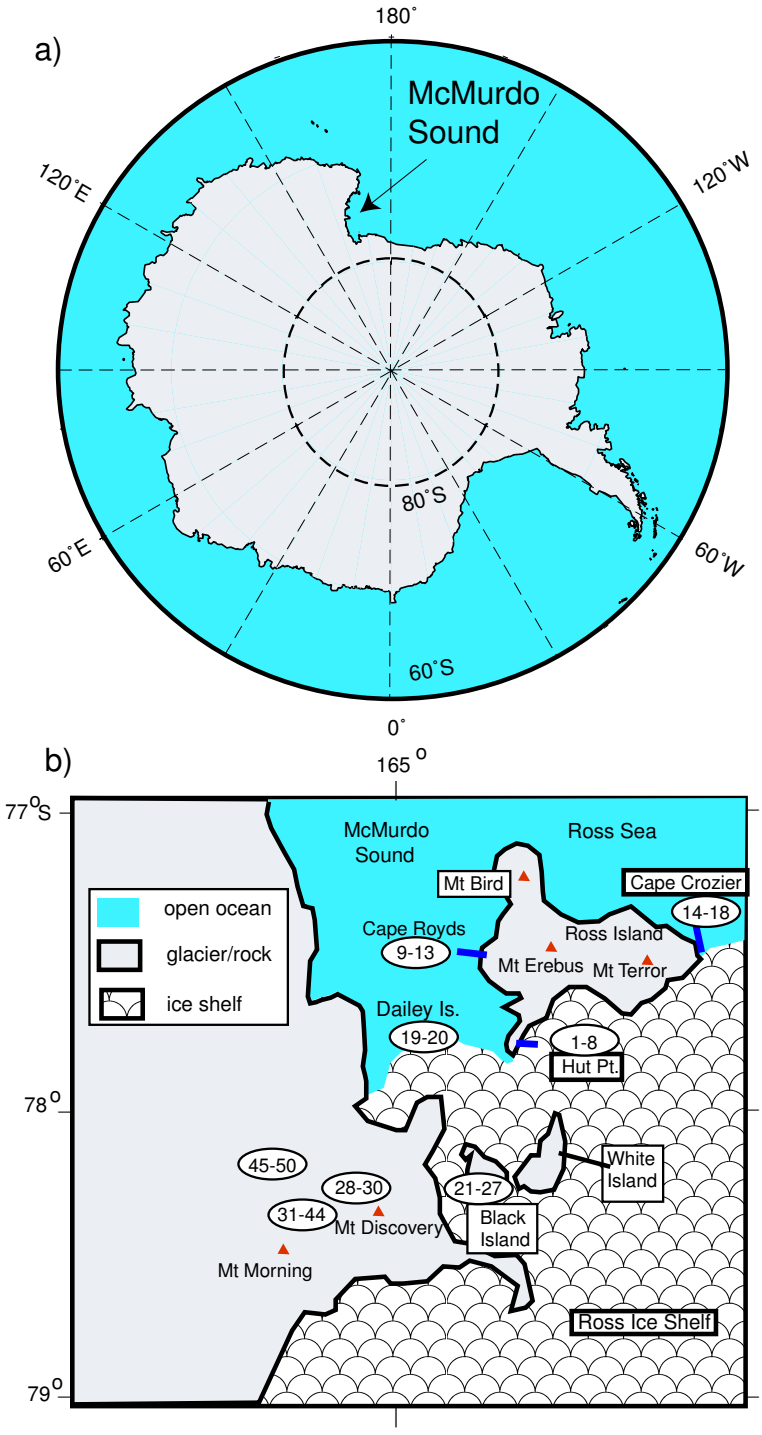

Figure 3. a) Map showing the location of McMurdo Sound on Antarctica. b) Map showing locations of the sampling sites.

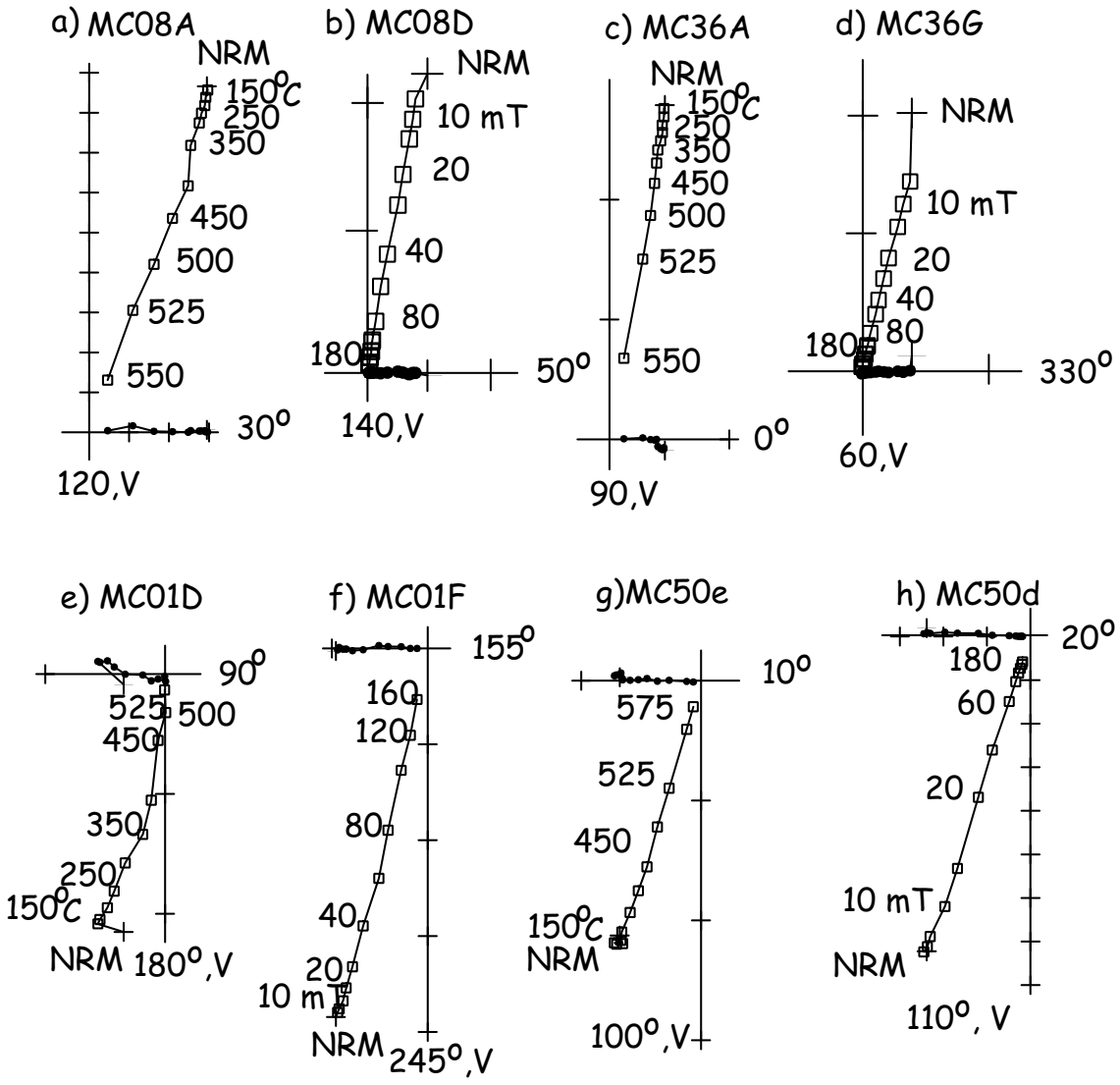

Figure 4. Orthogonal projections of representative specimens during thermal and AF demagnetization. Horizontal (vertical) projections are solid (open) symbols. The azimuths of the horizontal axes are noted.

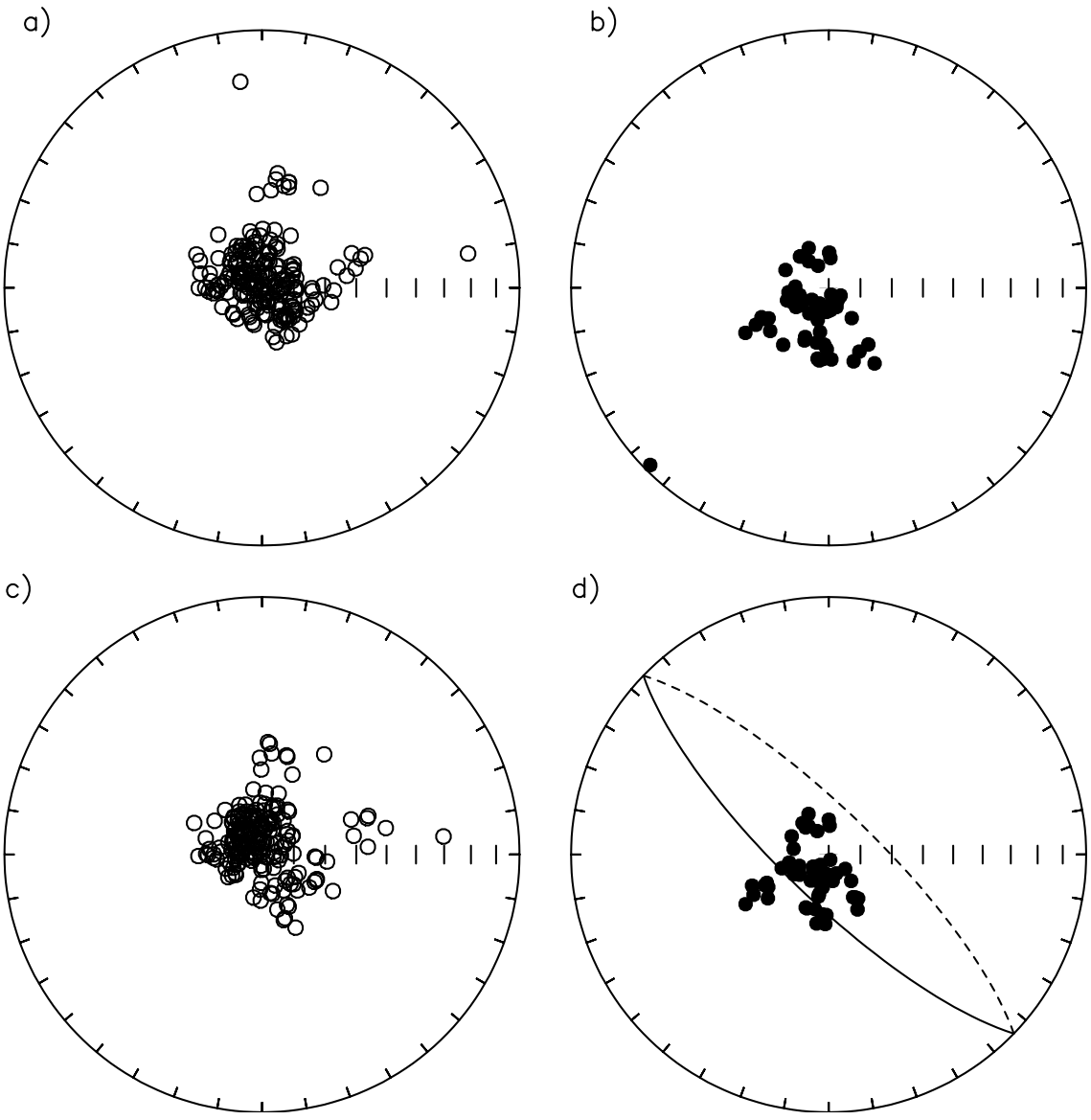

Figure 5. Equal area projections of specimen directions of the McMurdo Sound data set. Solid (open) symbols are lower (upper) hemisphere projections. a) NRM normal directions. b) NRM reverse directions. c) Directions of characteristic components from normal specimens. d) Directions of characteristic components from reverse specimens. Also shown is the best fit plane from one specimen.

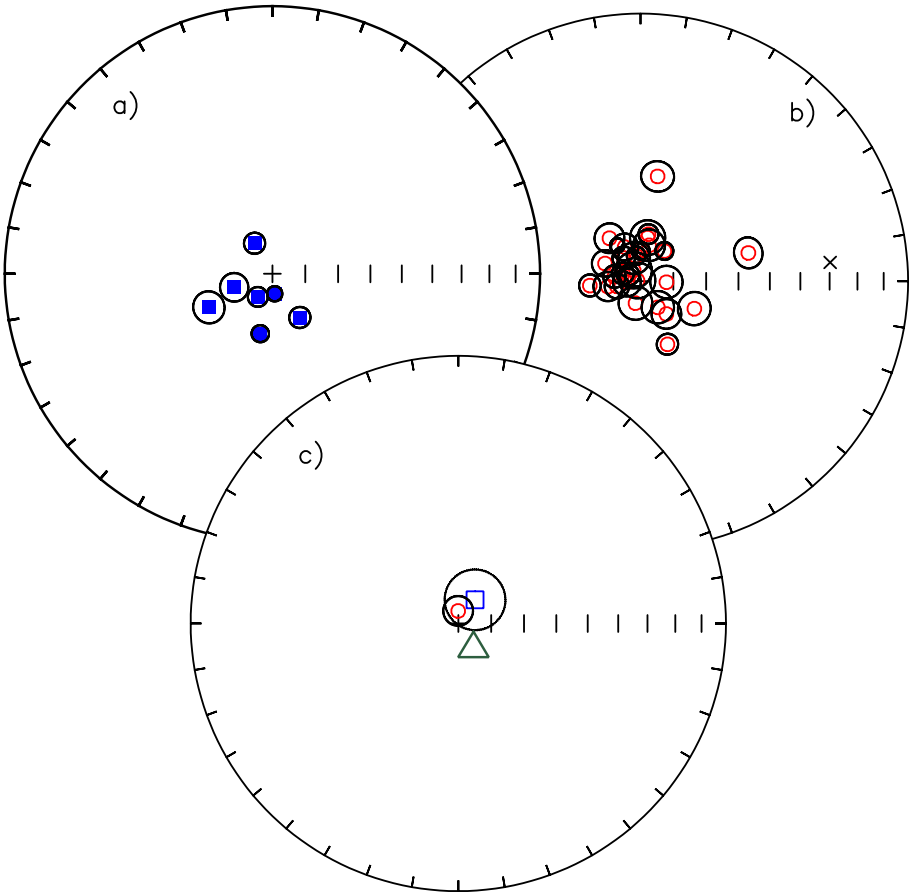

Figure 6. Equal area projections of directions of site means for the McMurdo Sound data set (Table 1). The 'X' is the upper hemisphere direction of the sole specimen from mc42 that yielded a best-fit line meeting minimum criteria. All other sites had $k \geq 100, N_{site} \geq 5$. a) Fisher (1953) mean directions with their 95% circles of confidence of the reverse sites. b) Same for normal sites means. c) Grand means of normal (circle) and the antipodes of the reverse sites (square) with 95% confidence ellipses. The two mean directions are indistinguishable at the 95% level of confidence. The triangle is the direction of the present field at McMurdo Sound. The expected direction from a GAD field is indistinguishable from the mean normal direction and is left off the plot for clarity.

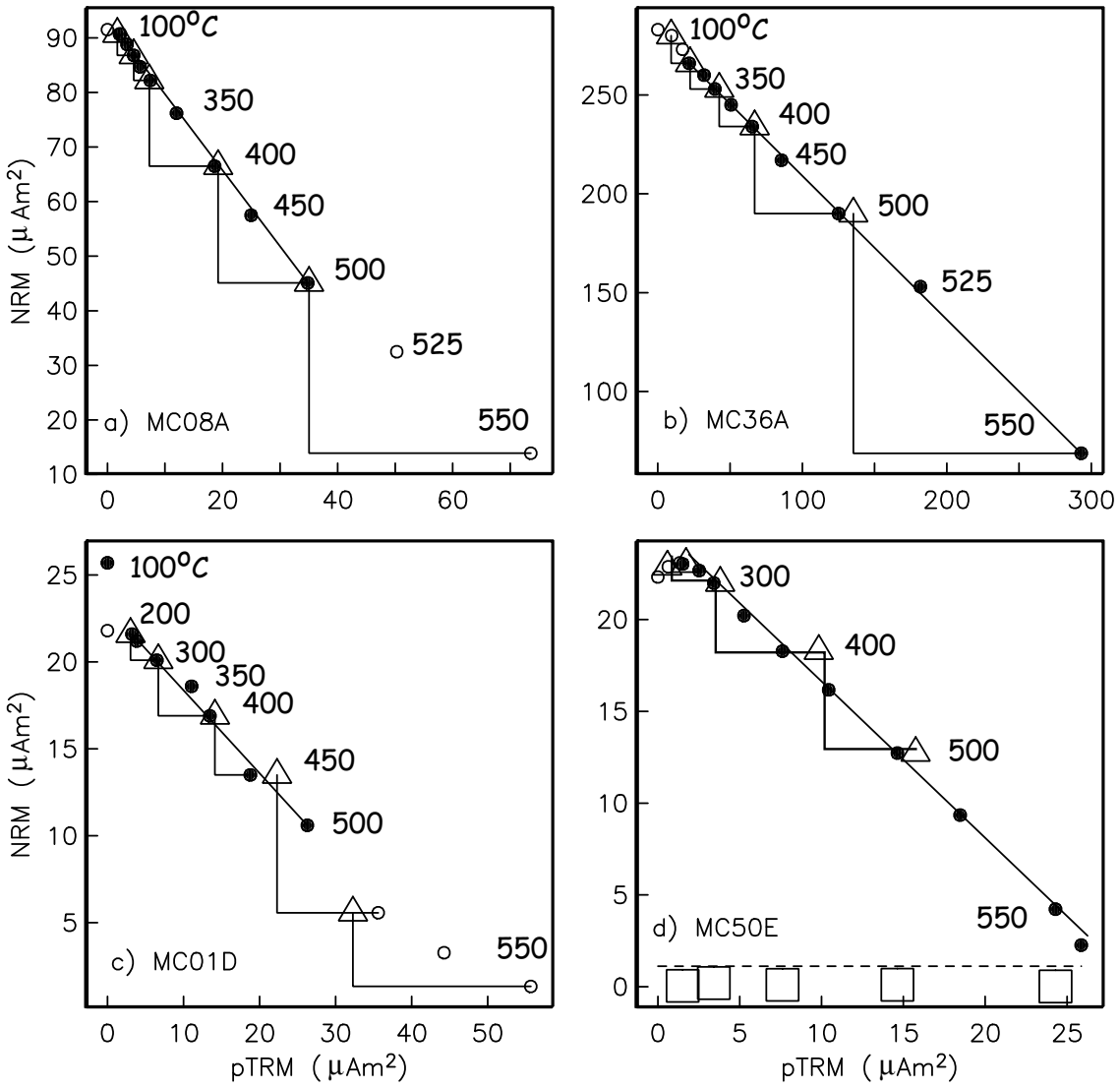

Figure 7. Representative results of successful Thellier-Thellier experiments. The associated vector diagrams are in Figure 4. The solid symbols are the data points used in the calculation of best-fit slope. Triangles are the "pTRM checks" and squares are the "pTRM tail checks". The dashed line in d) is the 5% level of reproducibility for the MD checks (see text).

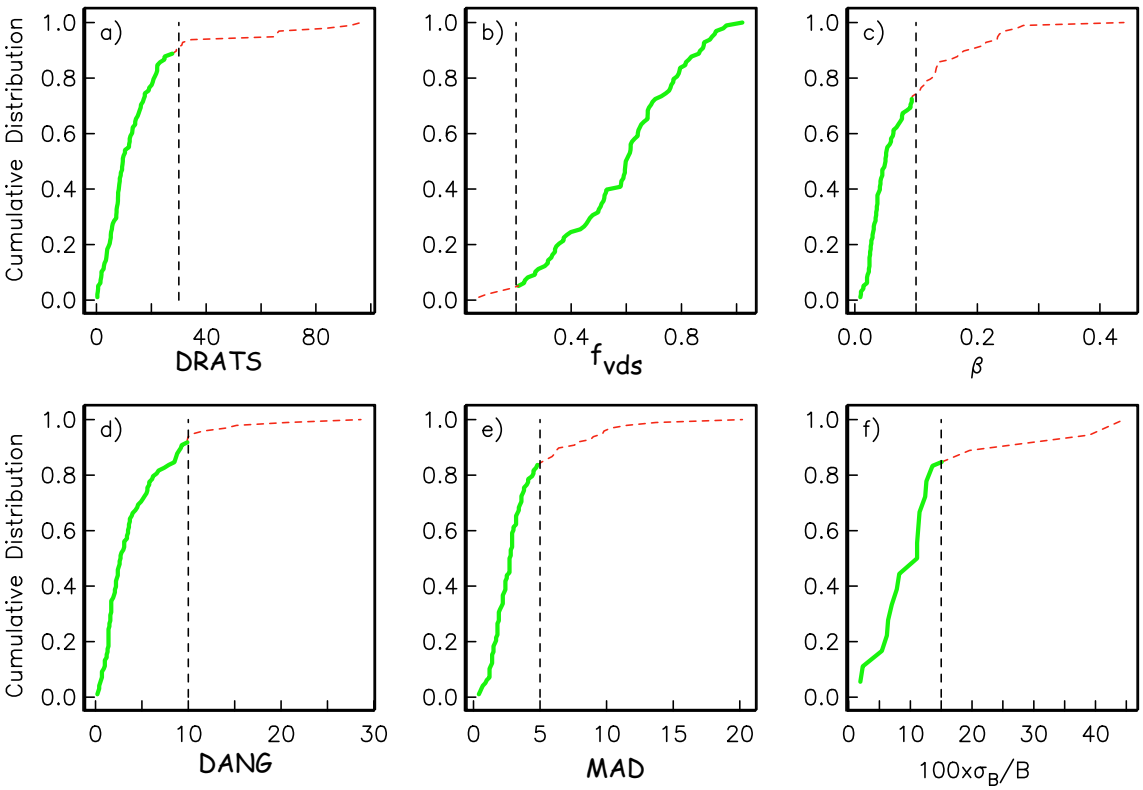

Figure 8. Cumulative distributions of various parameters from the Thellier-Thellier experiments. The dashed portions are considered "outliers" and are excluded from the calculation of site means. a) Difference Ratio Sum (DRATS). b) Fraction of the vector difference sum of the NRM f_{vds}. c) Standard error of the slope over the absolute value of the slope ($\sigma_b/|b| = \beta$). d) Deviation angle of the principal component from the origin, DANG. e) Maximum angle of deviation (MAD). f) Standard deviation of the mean of the site expressed as a percentage of the mean paleofield intensity.

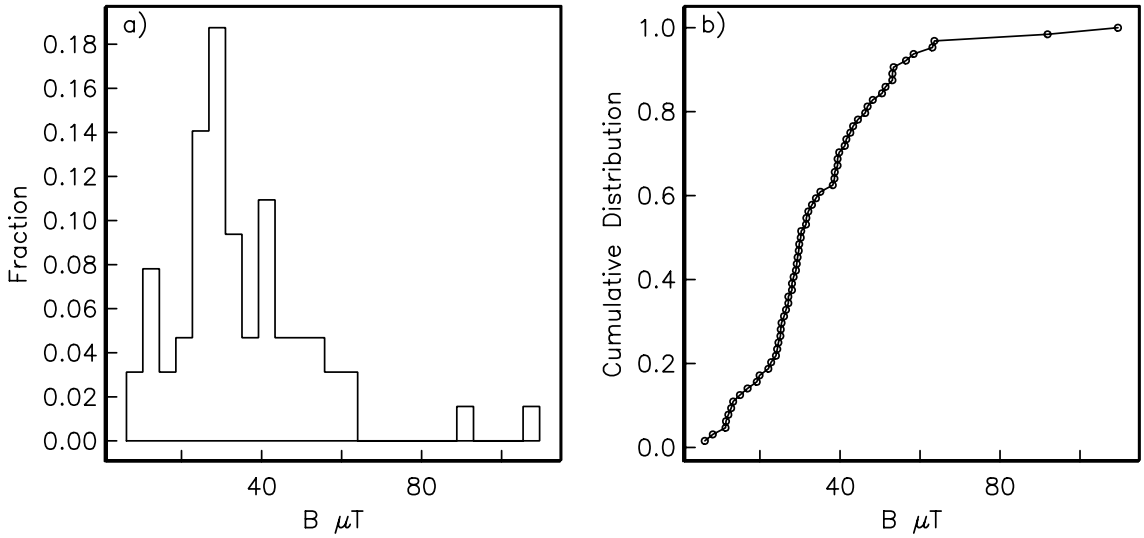

Figure 9. Distribution of paleointensity estimates from specimens meeting the minimum reliability criteria. a) Histogram. b) Cumulative distribution.

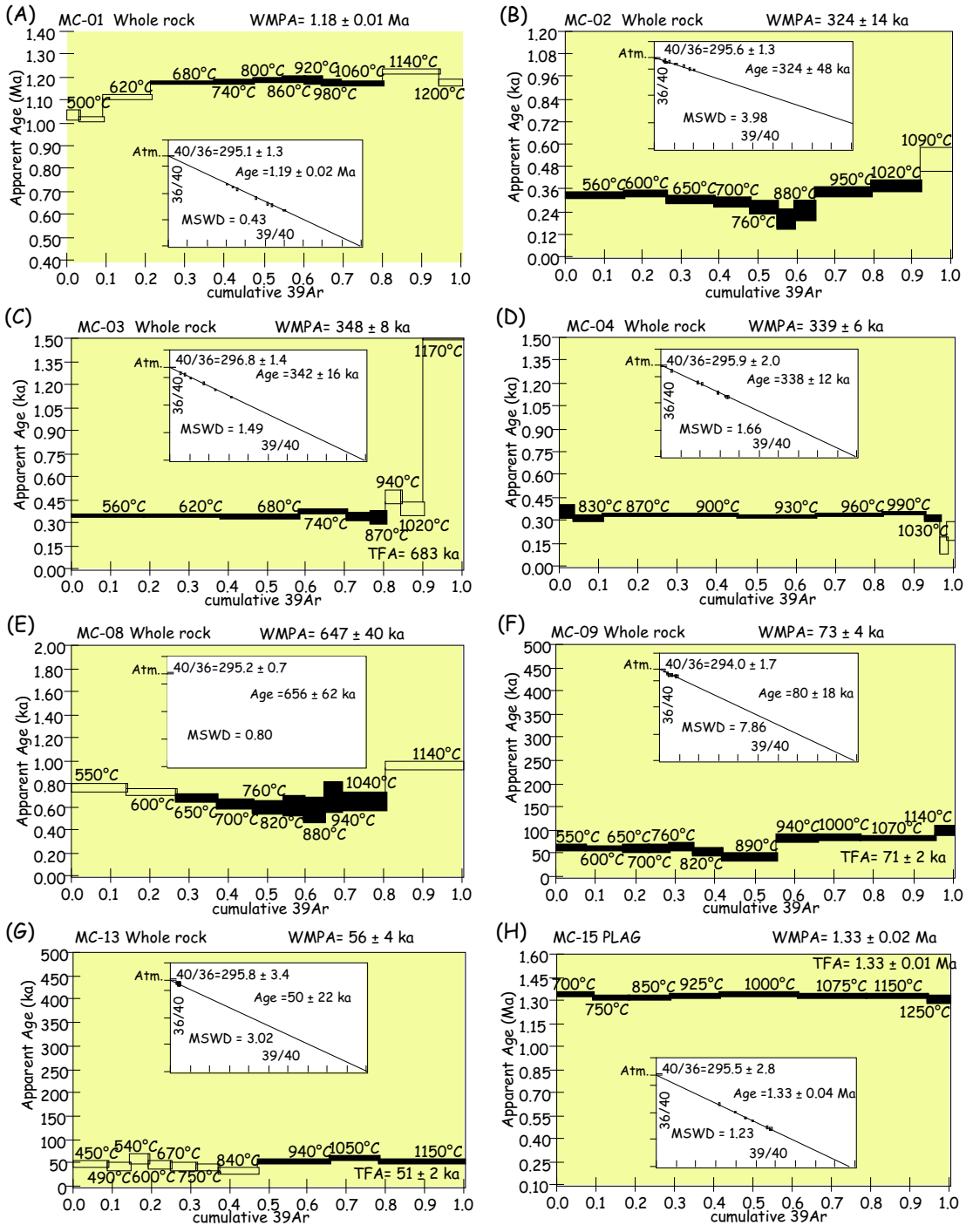

Figure 10. $^{40}Ar/^{39}Ar$ age spectra for selected paleomagnetic samples from the Hut Point Peninsula, Cape Royds, Cape Evans, Cape Crozier, and Dailey Island of the McMurdo Volcanic Province. All data from incremental heating experiments are plotted as apparent age of each temperature step versus the cumulative fraction of ^{39}Ar gas released. Steps used in the weighted mean plateau age calculation and are shaded black. Inset window for each sample depicts the inverse isochron plot with the calculated isochron age and $^{40}Ar/^{39}Ar$ ratio of the trapped component for the same data. Temperatures for each step are in °C. All errors (illustrated by each step thickness on the spectra and by the size of the boxes on the isochron plots) are estimated 1 σ errors without the error in J (flux parameter).

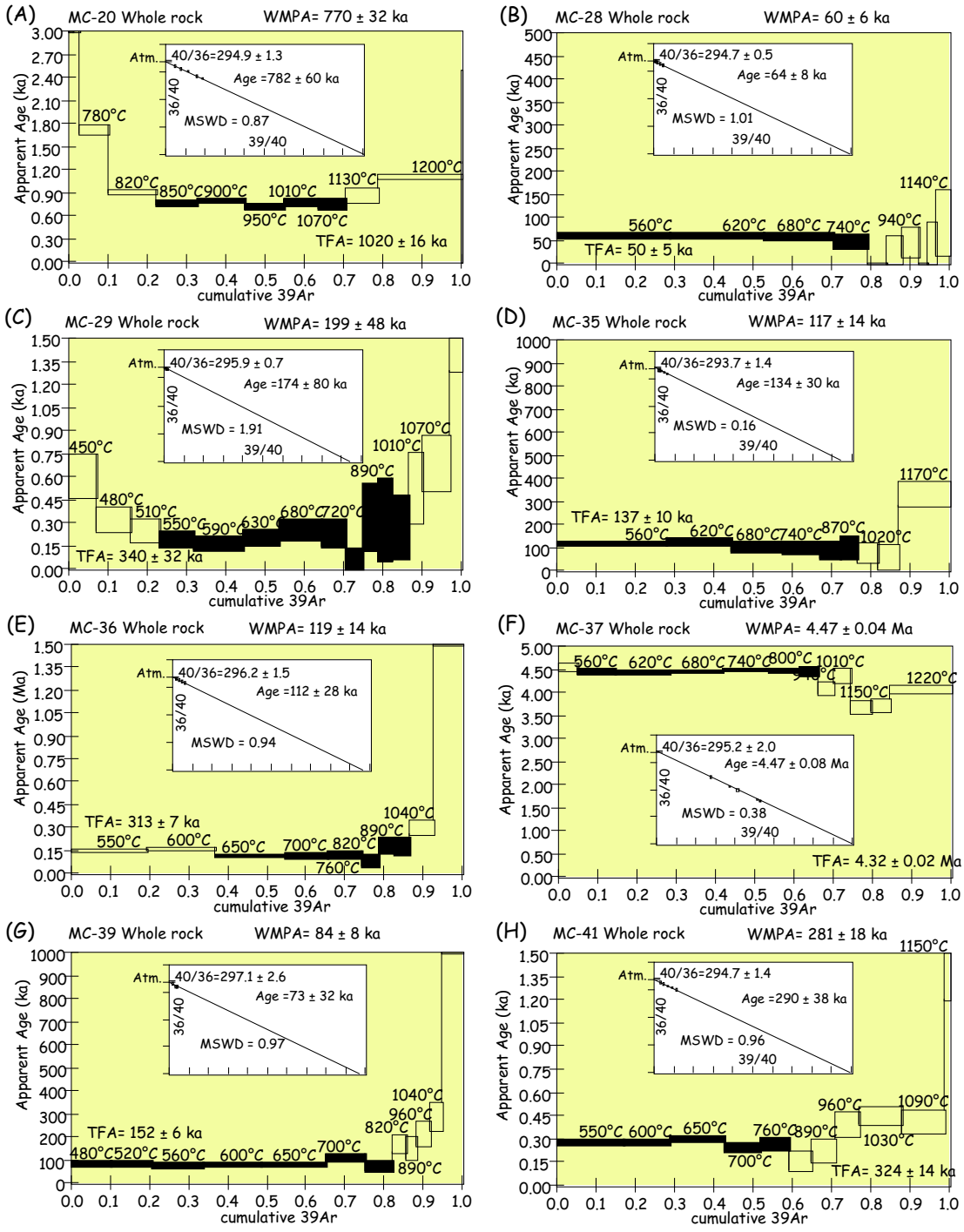

Figure 11. $^{40}Ar/^{39}Ar$ age spectra for selected paleomagnetic samples from the Mount Discovery and Mount Morning areas of the McMurdo Volcanic Province. See explanation for Figure 10.

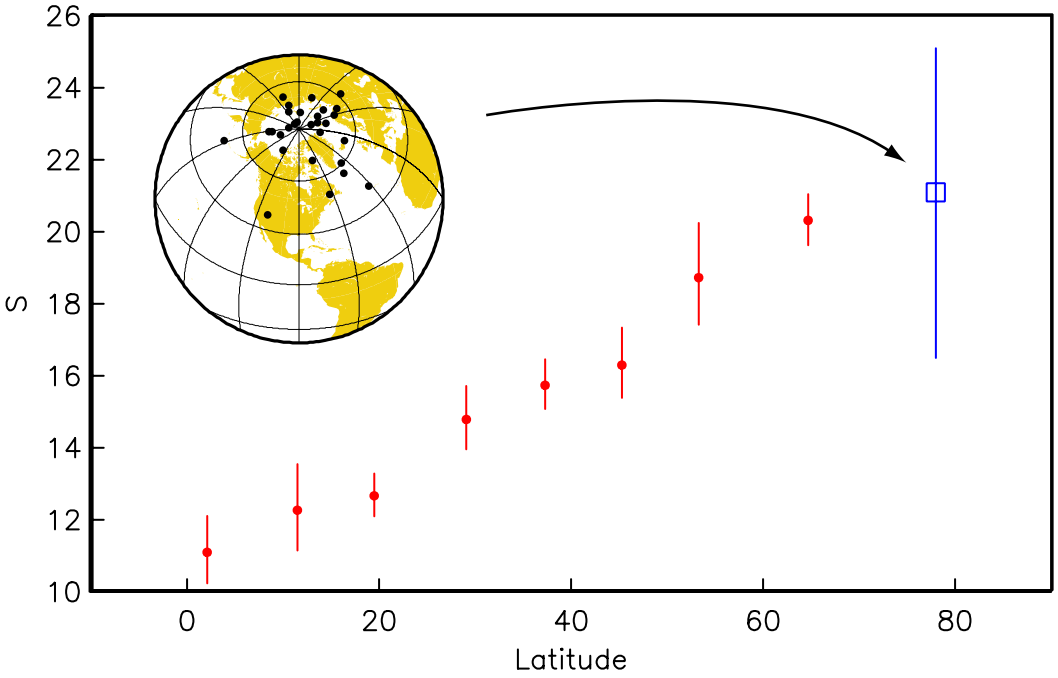

Figure 12. Solid symbols are the variation in scatter S of VGPs as a function of latitude estimated from the compilation of directions from lava flows spanning the last 5 m.y. of MM97. Vertical lines are the 95% confidence intervals. The square is from the data in the inset from McMurdo Sound. The inset is a map of the VGPs from Table 1 (excluding mc42). VGPs south of 48.5° were excluded by the Vandamme (1994) criterion for consistency with the MM97 estimates for S.

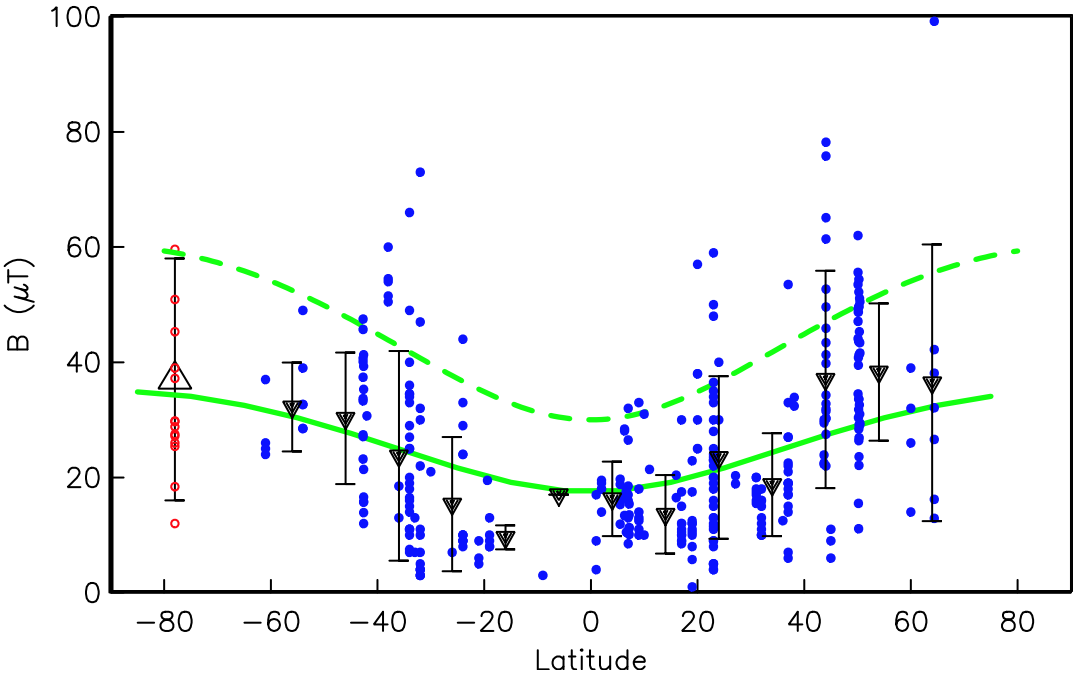

Figure 13. Closed symbols are the paleointensity data in the compilation of Selkin and Tauxe (2000) versus latitude of observation. Dots are individual cooling units and the triangles are the averages for 10° latitude bins. Open circles are the 15 cooling unit (site) means from McMurdo Sound listed in Table 2 meeting the minimum reliability criteria discussed in the text. The triangle is the mean. The solid line is the paleofield expected from the average dipole moment estimated for the last 5 million years by Selkin and Tauxe (2000) of 45.2 ZAm^2 and the dashed line is the intensity expected from the present dipole moment of 80 ZAm^2.